Received May 1, 2019, accepted June 13, 2019, date of publication June 26, 2019, date of current version July 18, 2019.

Digital Object Identifier 10.1109/ACCESS.2019.2925096

Feasibility Study of Limited-Angle Reconstruction for *in Vivo* Optical Projection Tomography Based on Novel Sample Fixation

NAN WANG, DUOFANG CHEN, DAN CHEN, CUIPING BAO, JIMIN LIANG, XUELI CHEN, (Member, IEEE), AND SHOUPING ZHU, (Member, IEEE)

Engineering Research Center of Molecular and Neuro Imaging, Ministry of Education, School of Life Science and Technology, Xidian University, Xi'an 710126, China

Corresponding authors: Xueli Chen (xlchen@xidian.edu.cn) and Shouping Zhu (spzhu@xidian.edu.cn)

This work was supported in part by the National Key R&D Program of China under Grant 2018YFC0910602, in part by the National Natural Science Foundation of China under Grant 81227901, Grant 81627807, Grant 81871397, and Grant 61471279, in part by the Fok Ying-Tong Education Foundation of China under Grant 161104, in part by the Program for the Young Top-notch Talent of Shaanxi Province, in part by the Research Fund for Young Star of Science and Technology in Shaanxi Province under Grant 2018KJXX-018, and in part by the Fundamental Research Funds for Central Universities under Grant JB171202, Grant JB171206, Grant JB181203, Grant JB181201, Grant XJS17049, and Grant JB191205.

ABSTRACT Optical projection tomography (OPT) is a novel three-dimensional imaging technique, which provides an approach to recreating the three-dimensional images of biological specimens ranging from millimeters to centimeters. In the current OPT setup, the specimen was immersed in the index-matching fluid. In this case, the specimen could not survive or the survival time was too short for longitudinal imaging. In this paper, we first designed a new type of sample fixation method for *in vivo* OPT imaging. The specimen was embedded into a transparent gel in a petri dish, and the dish was affixed to the rotational stage of our homemade OPT system. As the specimen does not need to be immersed in the index-matching fluid, this method can reduce the damage to the specimen and it is more conducive to longitudinal observation for *in vivo* OPT. However, this fixation method induces a problem of insufficient measurements. The angles parallel to or nearly parallel to the surface of the dish cannot be acquired. To address this problem, we, then, used a limited-angle reconstruction framework for the novel sample fixation-based OPT, which combines the algebraic reconstruction technique (ART) algorithm with prior information to solve the inverse reconstruction problem. The feasibility and effectiveness of the proposed sample fixation method and the limited-angle reconstruction framework were verified by the simulations and experiments.

INDEX TERMS Optical projection tomography, *in vivo* imaging, limited-angle reconstruction, sample fixation.

I. INTRODUCTION

Optical projection tomography (OPT) is an optical form of computer tomography, which recreates three-dimensional images by acquiring a series of two-dimensional, angle-dependent projection images of light intensity, and then using a reconstructed algorithm to recover the volumetric information of specimens. Compared with other popular imaging tools such as magnetic resonance imaging [1], micro computed tomography [2]–[4], synchrotron radiation-based X-ray tomography [5], optical coherence tomography [6], fluorescence molecular tomography [7], fluorescence microscopy [8], and multiphoton microscopy [9], [10], OPT can provide the micron-scale spatial resolution and the imaging depth of a few millimeters. Therefore, it has a great significance on the study of complex biological phenomena. In traditional OPT imaging, the specimen needs to be specially processed prior to performing the imaging experiment. Usually, the specimens were immersed in a mixture of benzyl alcohol and benzyl benzoate (Benzyl Alcohol: Benzyl Benzoate = 1:2, BABB) for reducing the photon refraction and scattering of biological tissues to maintain better spatial resolution [11], [12]. However, it is difficult to perform *in vivo* biological imaging. After the concept of *in vivo* OPT was

The associate editor coordinating the review of this manuscript and approving it for publication was Yunjie Yang.

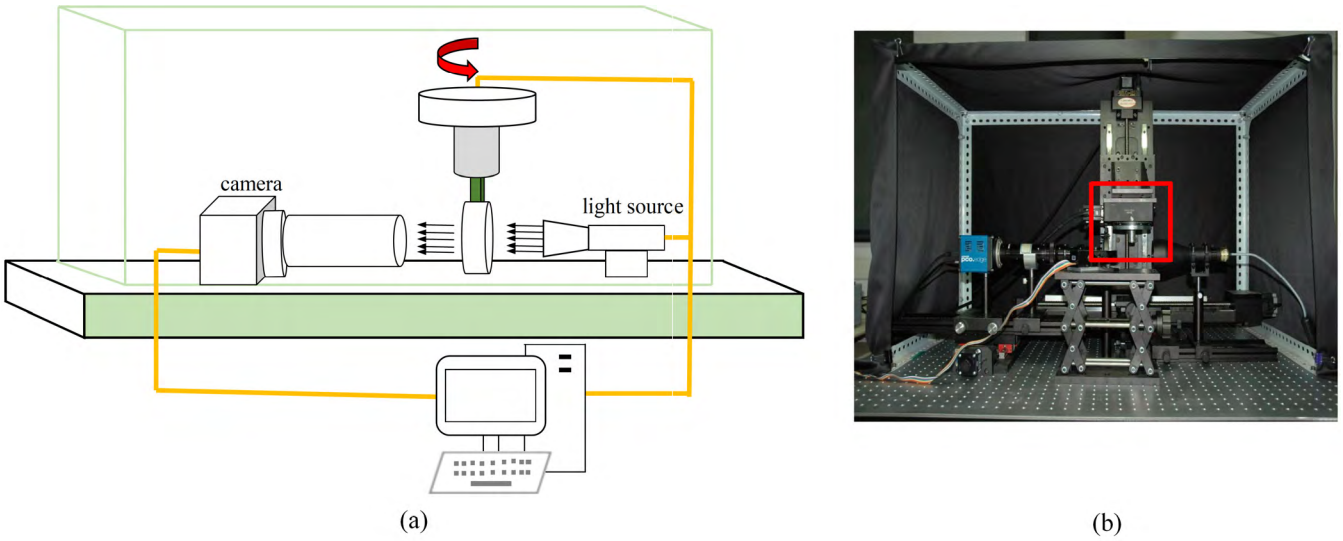

FIGURE 1. Homemade OPT system. (a) Schematic diagram. (b) Picture of the setup.

proposed, researchers put forward a sample fixation method that the specimen was placed in a capillary tube [13]–[15] or a Fluorinated Ethylene Propylene (FEP) tube [16]–[18] for realizing *in vivo* OPT, in which the tube was filled with a matching liquid to reduce the refractive index. In such ways, the imaged specimens only survived for several hours after a single experiment, failing to conduct longitudinal observation of the dynamics of the specimens.

To address this problem that *in vivo* OPT experienced, a novel sample fixation method was thus designed. In this method, the specimen was embedded in a petri dish and affixed to a transparent gel. The dish was then hung on the rotational stage of our homemade OPT system for *in vivo* imaging. Compared with conventional OPT imaging, the specimen does not need to be immersed in index-matching fluid in our proposed design. Thus, our method can reduce the damage to the specimen and be more conducive to the longitudinal observation for *in vivo* OPT imaging. Nevertheless, due to the geometry of the petri dish, the projections parallel or nearly parallel with the dish cannot be acquired. This means that we can only acquire the projection images at a certain, limited angle, which leads to the reconstruction problem of limited-angle tomography.

Limited-angle tomography has drawn much attention in many applications, such as X-ray computed tomography [19]–[25], mammography X-ray imaging [26], tooth tomography [27], and nondestructive detection of planar objects [28]. Due to many insufficient measurements, reconstruction of limited-angle tomography is seriously ill-posed. It is difficult to obtain satisfactory quality of images by either the traditional filtered back projection algorithm or algebraic reconstruction algorithm. Fortunately, during recent decades, great progress has been made in suppressing artifacts and improving image quality in the field of limited-angle tomography. These efforts can be divided into two categories. First is to compensate for the missing sinogram by extrapolation [29]–[31], and the other is to combine additional *a priori* information in the reconstruction process [32], [33]. *A priori* information about the unknown object, such as surface information, density range or the previous image, is helpful for artifact suppression and edge retention. Inspired by the theory of compressive sensing [34], *a priori* information of sparsity has drawn attention increasingly in the field of tomographic reconstruction. Such sparsity information could be utilized as the sparse regularization term which has been widely used in tomographic reconstruction. Total variation (TV) minimization algorithm, one of the widely used sparse regularization methods, has been successfully used for few-views and limited-angle data based tomographic reconstruction [20]. Therefore, we used TV regularization combined with the algebraic reconstruction technique (ART) to construct the limited-angle tomographic reconstruction framework in this paper. To reduce the errors caused by the projection operations in iterative reconstruction, a pixel vertex driven model (PVDM) that was derived from the separable footprint model [32] was designed and used to parallel-beam OPT in this work. The performance of the limited-angle reconstruction framework was first verified by numerical simulations. Experimental verifications were then conducted to demonstrate the feasibility and effectiveness of the novel sample fixation method and related limited-angle reconstruction framework.

II. MATERIALS AND METHODS

A. EXPERIMENTAL SETUP

Fig. 1 presents our homemade OPT setup, where Fig. 1(a) is a schematic diagram of the system, and Fig. 1(b) is the picture of the setup. It mainly contains four modules, including light source module, signal acquisition module, sample holding module, system control and data analysis module. In the light source module, a surface light source (BT-50*50SW, OSE, Singapore) was used to provide diffuse reflection light with

adjustable intensity. This light source is generally suitable for specimens with low transparency, such as living systems. In the signal acquisition module, an sCMOS camera (pco.edge 4.2, PCO, German) with high sensitivity, large dynamic range and low noise was selected as the detector. The sample holding module was comprised of a manually translational stage (PSMW 25A-65LL, Zolix, China), a high-precision rotational stage (ADRS100, Aerotech, USA), and three motorized linear translation stages (PSA200-11, Zolix, China). Among them, the manually translational stage was primarily used to position the sample as close as possible to the center of the rotational stage, allowing the sample to remain in the camera field of view. The high-precision rotational stage controls the sample rotation with adjustable rotation speed and step angle. Three motorized linear translation stages were used to adjust the position of the rotational stage in three directions. In the system control and data analysis module, we developed system control and data acquisition software for the OPT setup, including the functions of the system parameter setting and modification, controlling the translational and rotational stages, controlling the light source and detector, as well as data processing.

B. SAMPLE FIXATION FOR IN VIVO IMAGING

Currently, a capillary tube [13]–[15] or a Fluorinated Ethylene Propylene (FEP) tube [16]–[18] was used for sample fixation in *in vivo* OPT. Such a sample fixation method needs to use a matching liquid to reduce the refractive index, which is not suitable for *in vivo* imaging. Here, a novel sample fixation method was designed to overcome this limitation. In this method, a petri dish rather than a tube was utilized to hold the sample. Thus, the matching liquid can be avoided. Then, a low concentration agarose gel was used to affix the sample to the inside of the petri dish. Before performing OPT imaging, it is necessary to affix the petri dish to the rotational stage, as outlined as the red rectangle in Fig. 1(b). A circular magnet was utilized to clamp the edge of the petri dish onto the lower end of the metal cylinder below the rotational stage. Using this method, it can reduce the damage to the specimen and it is more conducive to the longitudinal observation for *in vivo* OPT.

C. LIMITED-ANGLE RECONSTRUCTION FRAMEWORK

Our sample fixation method can reduce the damage to the specimen and allow performing of the *in vivo* experiment. However, it also induced the limited-angle tomographic problem. Due to the limitation of the geometry of the petri dish, instead of complete 360 projection images, only few or fewer projection images can be acquired. Fig. 2 shows the schematic of full- and limited-angle data acquisition respectively. Inspired by the theory of compressive sensing [34], Sidky *et al.* [20] proposed an image reconstruction algorithm called the total variation (TV) minimization algorithm to reconstruct the projection data from few-views and limited-angle data. Thus, here we constructed the limited-angle

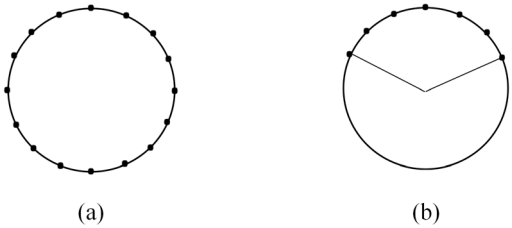

FIGURE 2. Schematic of full- and limited-angle imaging. (a) Full-angle sampling. (b) Limited-angle sampling.

reconstruction framework based on the TV minimization algorithm.

We assume that $f_{s,t}$ represents the gray value of the image, and the image gradient magnitude can be described as:

$$\left|\vec{\nabla} f_{s,t}\right| = \sqrt{(f_{s,t} - f_{s-1,t})^2 + (f_{s,t} - f_{s,t-1})^2} \tag{1}$$

In order to take advantage of the sparse property, the l_1-norm of the gradient image is taken as the minimized objective function, also called the full variation of the image.

$$\left\|f_{s,t}\right\|_{TV} = \sum_{s,t} \left|\vec{\nabla} f_{s,t}\right| = \sum_{s,t} \sqrt{(f_{s,t} - f_{s-1,t})^2 + (f_{s,t} - f_{s,t-1})^2} \tag{2}$$

The OPT imaging process can be described by the following linear model:

$$g_i = \sum_{j=1}^{N} w_{ij} f_j, \quad i = 1, \ldots, N_g \tag{3}$$

where f_j represents the pixel value of the j^{th} pixel of the image, and N represents the total number of pixels in the image. i is the index of the ray, and g_i represents the projection value of the i^{th} ray. N_g represents the total number of rays. w_{ij} represents the weight of the j^{th} pixel contributing to the magnitude of the i^{th} ray.

Equation (3) can be converted into a matrix form as:

$$\vec{\mathrm{g}} = \mathbf{W}\vec{f} \tag{4}$$

where $\mathbf{W}$ is a weight matrix. $\vec{\mathrm{g}}$ is the observed projection data, and the process of three-dimensional reconstruction is used to solve $\vec{f}$ by using the algebraic reconstruction technique (ART). The process of the iterative solution of ART is described below [35], [36]:

$$\vec{f}^{(k+1)} = \vec{f}^{(k)} + \lambda \vec{w}_i^T \frac{\mathrm{g_i} - \vec{\mathrm{w}}_i \vec{f}^{(k)}}{\left\|\vec{\mathrm{w}}_i\right\|^2} \tag{5}$$

where $\vec{\mathrm{w}}_i$ is the weight of the contribution of the pixels to the i^{th} ray and it is a $1\times$ N vector. $\vec{f}^{(k)}$ is an N $\times 1$ image vector and represents the reconstructed image of the kth iterative. λ represents the relaxation factor of the iteration. It speeds up the convergence of the algorithm and effectively overcomes noise during the iteration. In general, $0 < \lambda \leq 1$.

Since the light attenuation coefficient of an object cannot be negative, a non-negative constraint was applied to the

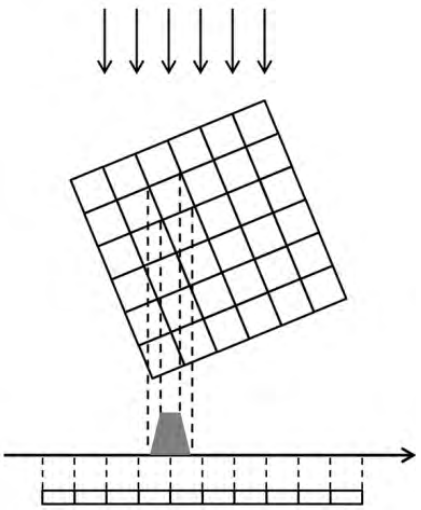

FIGURE 3. Diagram of the pixel vertex driven model for the parallel illumination.

ART algorithm to speed up the iteration and improve the reconstructed image quality:

$$f_j = 0, \quad \text{if } f_j < 0 \tag{6}$$

The minimum image total variation (TV) is used as the optimization criterion of the iterative reconstruction. The TV based minimization problem was solved by the steepest descent method, which is defined as [20]:

$$\begin{aligned} d_{s,t} = \frac{\partial \left\|\vec{f}\right\|_{TV}}{\partial f_{s,t}} \approx & \frac{2f_{s,t} - f_{s-1,t} - f_{s,t-1}}{\sqrt{\varepsilon + (f_{s,t} - f_{s-1,t})^2 + (f_{s,t} - f_{s,t-1})^2}} \\ & - \frac{f_{s+1,t} - f_{s,t}}{\sqrt{\varepsilon + (f_{s+1,t} - f_{s-1,t})^2 + (f_{s+1,t} - f_{s+1,t-1})^2}} \\ & - \frac{f_{s,t+1} - f_{s,t}}{\sqrt{\varepsilon + (f_{s,t+1} - f_{s-1,t})^2 + (f_{s,t+1} - f_{s-1,t+1})^2}} \end{aligned} \tag{7}$$

In general, the solution steps of the TV minimization based ART algorithm can be described as follows:

Algorithm

1. Initialization. $\vec{f} = 0$ and $\vec{f}_0 = \vec{f}$;
2. Performing an ART iteration reconstruction with a projection model;
3. Non-negative constraints.
$$f_j = 0, \quad \text{if } f_j < 0$$
4. Calculation.
$$d_{img} = \left|\vec{f} - \vec{f}_0\right|$$
5. Performing the following TV minimization operations N_{grad} times.
Calculating $\vec{d}$ and its unit vector $\hat{d}$ according to (7).
Image update:
$$\vec{f} = \vec{f} - \lambda_{TV} d_{img} \hat{d}$$
6. $\vec{f}_0 = \vec{f}$
7. $\lambda = \lambda \times 0.99$
8. Determine whether the stop criterion is met. If it meets the conditions, stop the iteration. Otherwise, go to step 2 to perform the next iteration.

There are several parameters which are very important for reproducing the results, including relaxation factor λ, iteration number N_{grad} of TV, regularization parameter λ_{TV} and iteration number N of ART. These parameters can be empirically determined [21], [20], [37], [38]. In our experiments, we set them as: $\lambda = 1$, $N_{\text{grad}} = 10$, $\lambda_{TV} = 0.08$ and $N = 50$.

In order to reduce the errors of forward and back projections in iterative reconstruction, we designed a pixel vertex

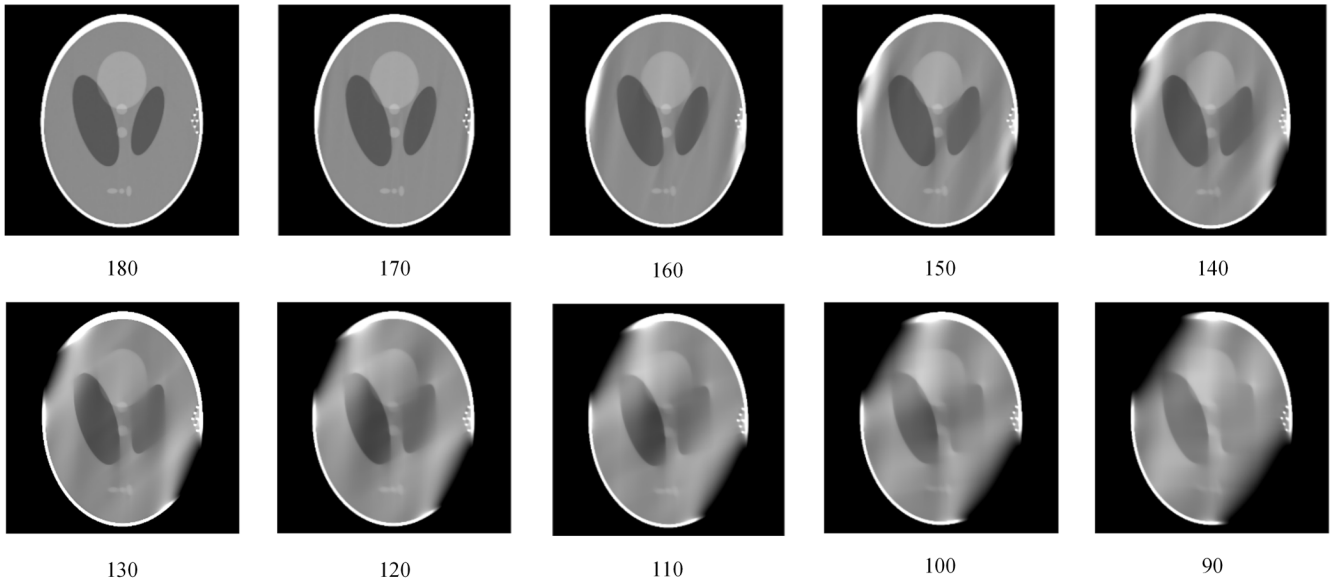

FIGURE 4. Reconstructed images via the TV based ART algorithm using different angular ranges.

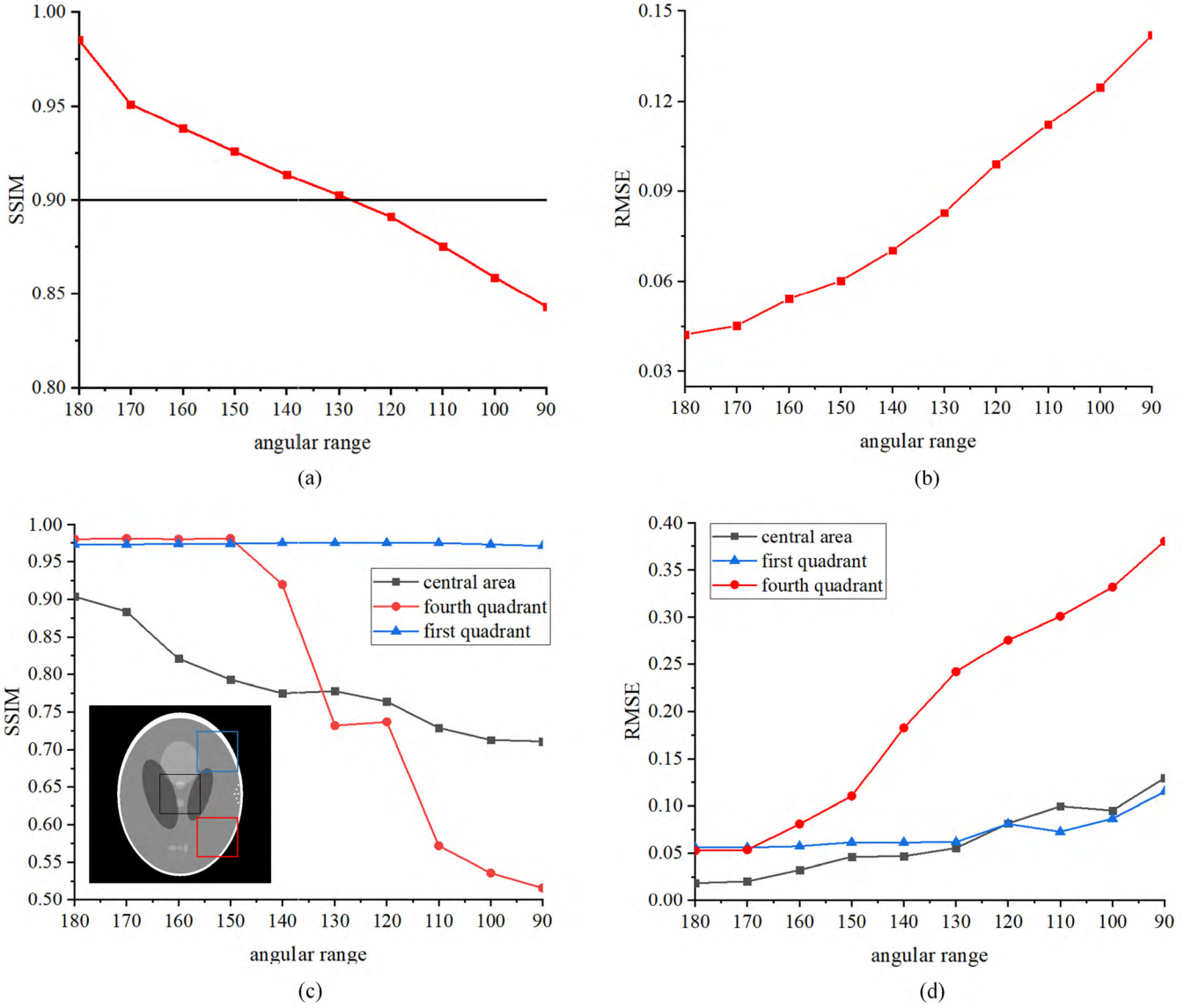

FIGURE 5. Quantitative evaluations. (a) SSIM values as a function of angular range. (b) RMSE values as a function of angular range. (c) SSIM values of different area of reconstructed images. (d) RMSE values of different area of reconstructed images.

driven model (PVDM) which is borrowed from the separable footprint model used in cone-beam CT [39]. Here, we made some modifications so that they can be applied to parallel-beam OPT. Fig. 3 shows the diagram of the PVDM model for parallel illumination. The projection model projects four vertices of the pixel along the direction from the light source to the detector. According to the position of the four vertices after the pixel is projected, the overlap of the projection and the detector can be determined, which acts as the weight.

D. SAMPLE PREPARATION

The sample used here was *Nicotiana benthamiana*, which was cultivated in a constant temperature incubator. During the experiment, the lobular tobacco seeds were selected and sterilized by using 75% alcohol for 30 s before culturing, and then washed three times with sterile water for 30 s each time. After drying on sterile filter paper, it was placed in a petri dish containing 2/3 volume of MS solid medium, with one plant per dish. The petri dish was then sealed with parafilm at the end of seeding to maintain moisture. The cells were placed in a thermostatic light incubator at a horizontal temperature for 16 h light (28°) and 8 h dark (25°). When obvious root hairs appeared, we carried out the OPT experiment on *Nicotiana benthamiana*.

E. EVALUATION INDEX

In order to quantitatively evaluate the reconstruction results, we used structural similarity (SSIM) and root mean square error (RMSE) to evaluate the quality of these reconstruction results. SSIM is a widely used image quality evaluation index, which was proposed by Wang et al. in 2004 [40]:

$$SSIM(X,Y)=\frac{2\mu_X\mu_Y+C1}{\mu_X^2\mu_Y^2+C1}\cdot\frac{2\sigma_X\sigma_Y+C2}{\sigma_X^2\sigma_Y^2+C2}\cdot\frac{\sigma_{XY}+C3}{\sigma_X\sigma_Y+C3} \tag{8}$$

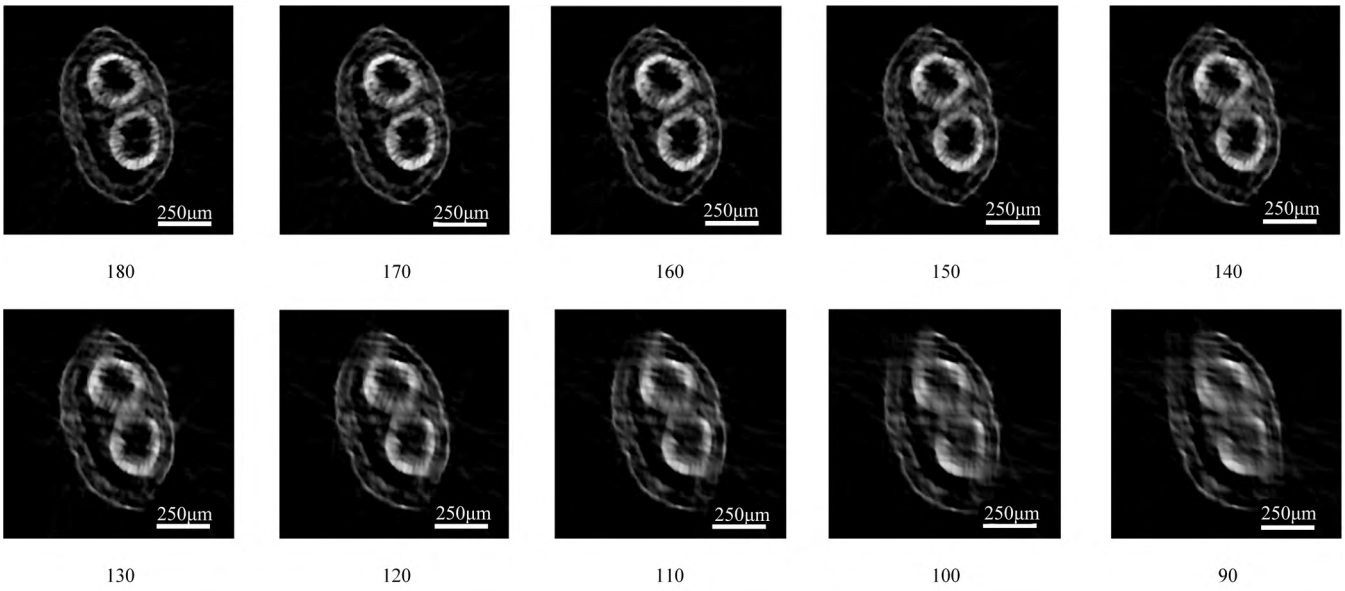

FIGURE 6. Reconstructed *Arabidopsis silique* images of the TV based ART algorithm by using different projections from angular ranges of 180 170, 160, 150, 140, 130, 120, 110, 100, and 90 degrees.

Eq.(8) is the correlation function of brightness, contrast and structure of the two images, where X and Y represent the two images being compared. μ_X, μ_Y represent the mean values of image X and Y respectively. μ_X, μ_Y represents the variance of images X and Y. σ_{XY} represents the covariance of images X and Y. $C1$, $C2$ and $C3$ are the constants. The SSIM value ranges from 0 to 1. The closer the SSIM value is to 1, the higher the similarity between the two images.

RMSE is a frequently used index to evaluate the deviation extent of the reconstructed data from the true values. The smaller the value, the more accurate the reconstructed image. It can be calculated as follows [22]:

$$RMSE = \sqrt{\sum_{x,y} (C_{x,y} - C^*_{x,y})^2 / N} \tag{9}$$

where $C_{x,y}$ and $C^*_{x,y}$ represent the values of the reconstructed image and the true image in pixel (x, y), and N is the pixel number of the region we are interested in.

III. EXPERIMENT AND RESULTS

A. SIMULATIONS

The validity of the TV based ART algorithm for limited-angle reconstruction of OPT was first evaluated with simulations. A modified Shepp-Logan model [41] was used as the physical model to generate full angle projection images. The forward projection images were generated by using a pixel vertex driven model. In the evaluation, different projections with intervals of 1° were sampled from different angular ranges consisting of 180, 170, 160, 150, 140, 130, 120, 110, 100, and 90 degrees. The sinogram maps of these projection images were reconstructed with the TV based ART algorithm. The original image and the reconstructed image from 180 degrees are shown in Supplementary Figure S1. Fig. 4 shows the reconstructed images via the TV based ART algorithm using different angular ranges. We observed that the image distortion became more and more serious as the angular range decreased. In addition, the artifacts in the second and fourth quadrants are more obvious than other regions as the angular range decreased. This is because the direction of the projections was from the positive X-axis and counterclockwise rotation around the origin in the simulation experiment, as is shown in Supplementary Figure S1.

To quantitatively evaluate the quality of the reconstructed images, we used the original image as a standard to calculate the SSIM and RMSE values. Fig. 5(a) and Fig. 5(b) present the SSIM and RMSE values as a function of the angular range respectively. We determined that the SSIM value increased and RMSE value decreased with an increase in the angular range. When the angular range was 180 degrees, the SSIM value was 0.985 and the RMSE value was 0.042. When the angular range decreased to 90 degrees, the SSIM value was down to 0.843 and the RMSE value was 0.142. When the angular range was larger than 130 degrees, SSIM was >0.9.

Furthermore, in order to evaluate the quality of the reconstruction of the different regions, we selected different areas of the image to calculate the values of SSIM and RMSE. The selected areas were outlined in Fig. 5(c), including the central area outlined with a black square, the first quadrant with a blue square, and the fourth quadrant with a red square. Fig.5(c) and Fig.5(d) show the SSIM and RMSE values of different areas as a function of the angular range respectively. The change of SSIM values in the central area was similar to the SSIM change calculated overall for the whole image. Unlike the overall SSIM trend for the whole image, it changed slightly when the angular range was from 120 to 150 degrees in the central area. From the RMSE curves, we can also observe that the errors changed slightly as the angular range decreased. Since the area in the first

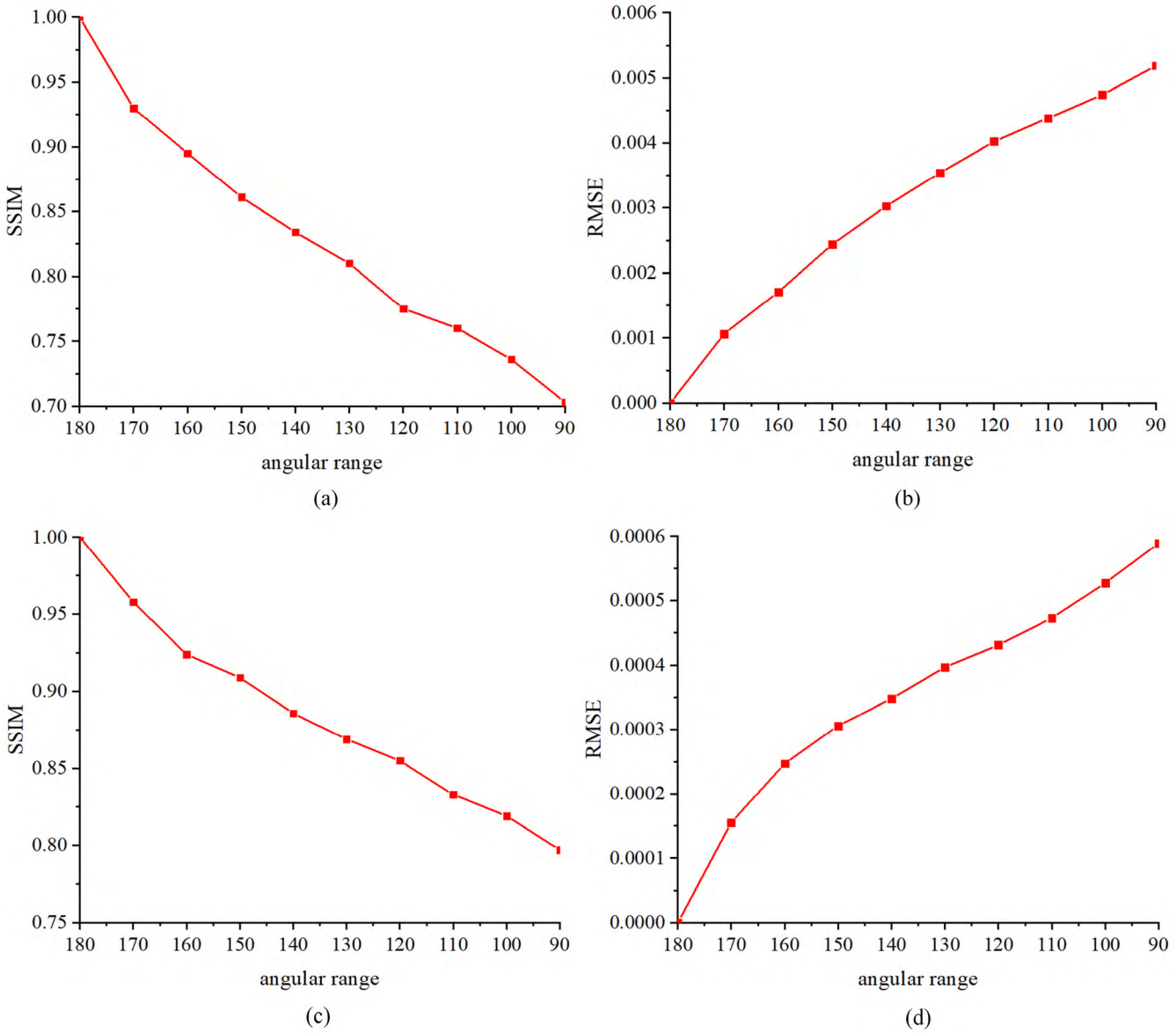

FIGURE 7. SSIM and RMSE values as a function of angular range. (a) SSIM values of *Arabidopsis silique*. (b) RMSE values of *Arabidopsis silique*. (c) SSIM values of *Drosophila*. (d) RMSE values of *Drosophila*.

quadrant changed slightly as the angular range decreased, almost no information was missing in this area with the SSIM values being over 0.97 and RMSE values being below 0.1. However, in the fourth quadrant, the SSIM values decreased and RMSE values increased dramatically when the angular range was below 140 degrees, whereas they changed slightly when the angular range was between 150 and 180 degrees. These results showed that the artifacts in the fourth quadrant are more serious and the fourth quadrant loses the most information as the angular range decreased.

B. EXPERIMENTAL VALIDATION

To further estimate the TV based ART algorithm for limited angle reconstruction of OPT, two biological experiments were performed. In the first biological experiment, *Arabidopsis silique* was used as the imaging sample. About 180 projections were acquired in an angular range of 180 degrees with an interval of 1° using our homemade OPT system. One of the projection images is presented in Supplementary Figure S2(a), and the image reconstructed by the TV based ART algorithm using 180 projection images is shown in Supplementary Figure S2(b). In the reconstruction algorithm, the number of ART iterations was set to 50, and the number of TV minimization iterations of N_{grad} was set to 10. To observe the degradation of image quality more intuitively and emphatically, we selected one section of the reconstructed volume and chose a region of interest (ROI, outlined with a red rectangle in Supplementary Fig. S2(c)) for analysis. Fig. 6 shows the reconstructed images of the TV based ART algorithm by using different angular ranges.

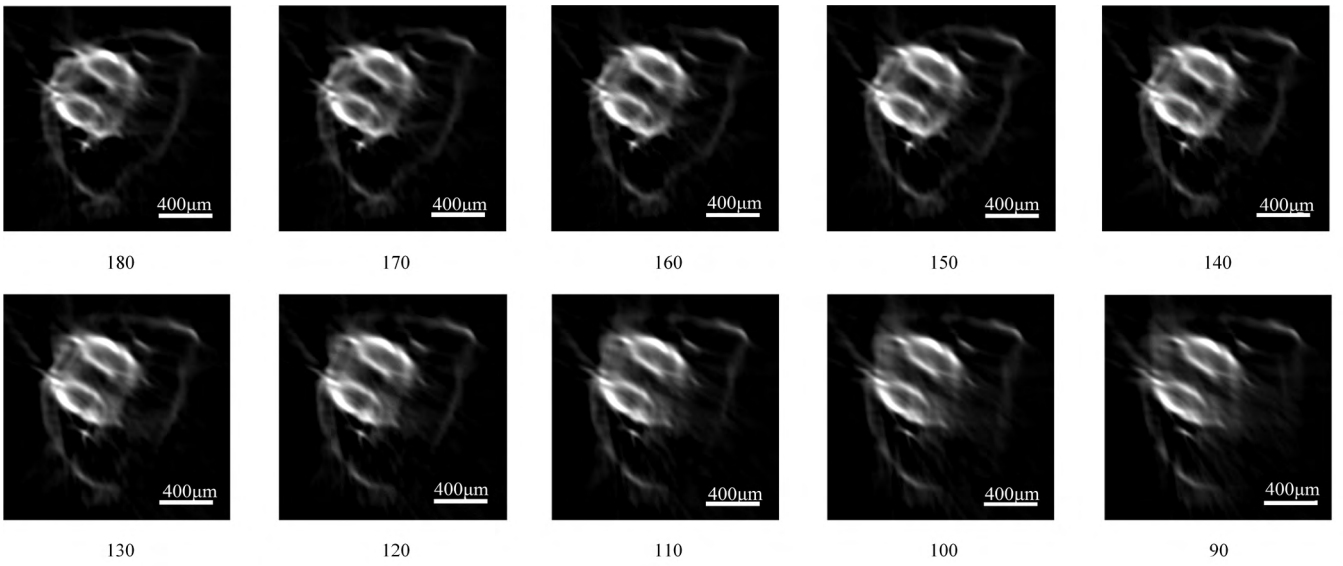

FIGURE 8. Reconstructed *Drosophila* images of the TV based ART algorithm by using different projections from angular ranges of 180, 170, 160, 150, 140, 130, 120, 110, 100, and 90 degrees.

In these images, there are two circles at the central region, which are two ovules of *Arabidopsis silique*. The ovules are surrounded by the pod wall. Similar conclusion to the simulation can be addressed. From Fig. 6, we found that the image quality became worse as the angular range decreased. When the angular range was greater than 140 degrees, the shape of the ovules did not change substantially. The shape of the ovules changed slightly when the angular range was between 120 and 140 degrees. However, when the angular range was less than 110 degrees, the ovules experienced serious distortion.

In order to quantitatively evaluate the quality of the reconstructed images, the SSIM and RMSE values as a function of angular range were also calculated and are shown in Fig. 7(a) and Fig. 7(b). It should be noted that there was no original image in the actual experiments. Thus, the reconstructed image of the TV based ART algorithm by using 180 projections was used as the standard in the actual imaging experiments. The SSIM curve descended and the RMSE curve ascended as the angular range decreased, which indicated the quality of the reconstructed image degraded correspondingly. When the angular range decreased to 170 degrees, the SSIM value was down to 0.93 and the RMSE value was 0.0011. However, when the angular range was down to 90, the SSIM value was as worse as 0.70 and the RMSE value increased to 0.0052.

In the second biological experiment, *Drosophila* in the pupa stage was selected as the imaging sample, and the same parameters and conditions were set as the first biological experiment. One projection image of *Drosophila* is shown in Supplementary Figure S3(a), and the reconstructed image of the TV based ART algorithm by using the angular range of 180 degrees is shown in Figure S3(b). Supplementary Figure S3(c) depicts one cross-sectional view of *Drosophila* at the 1435th layer. Similarly, we chose the ROIs in the sectional image for further analysis, as outlined with a red rectangle in Supplementary Figure S3(c). Fig.8 shows the reconstructed images of the TV based ART algorithm by using different angular ranges. In each image, there are two ovals which are the eyes of *Drosophila*. The thin layer outside is the outer shell of the pupa. Similar results as the simulation of the first biological experiment were obtained. The image quality became worse as the angular range decreased. When the angular range was greater than 120 degrees, the shape of *Drosophila* eyes changed slightly. Conversely, when the angular range was less than 110 degrees, the eyes of *Drosophila* were severely deformed, especially in the relative positions between other tissues and the eyes of *Drosophila*. Fig.7(c) and 7(d) show the SSIM and RMSE values as a function of angular range. We found that the SSIM values were reduced and RMSE values were increased almost linearly as the angular range decreased, indicating that the reconstructed images became gradually worse. When the angular range was 170 degrees, the SSIM value was 0.96 and the RMSE value was 0.0002. However, when the angular range was reduced to 90, the SSIM value was down to 0.80 and the RMSE value was 0.0006. These results were nearly consistent with the results of the *Arabidopsis silique* experiment.

Both of the biological experiments demonstrated that the TV based ART algorithm provided promising performance when the angular range was no smaller than 140 degrees, and provided acceptable performance when the angular range was larger than 110 degrees. In our proposed petri dish based sample fixation method, due to the geometry limitation, the maximum angular range that could be used for image acquisition was 140 degrees. Thus, the TV regularized ART

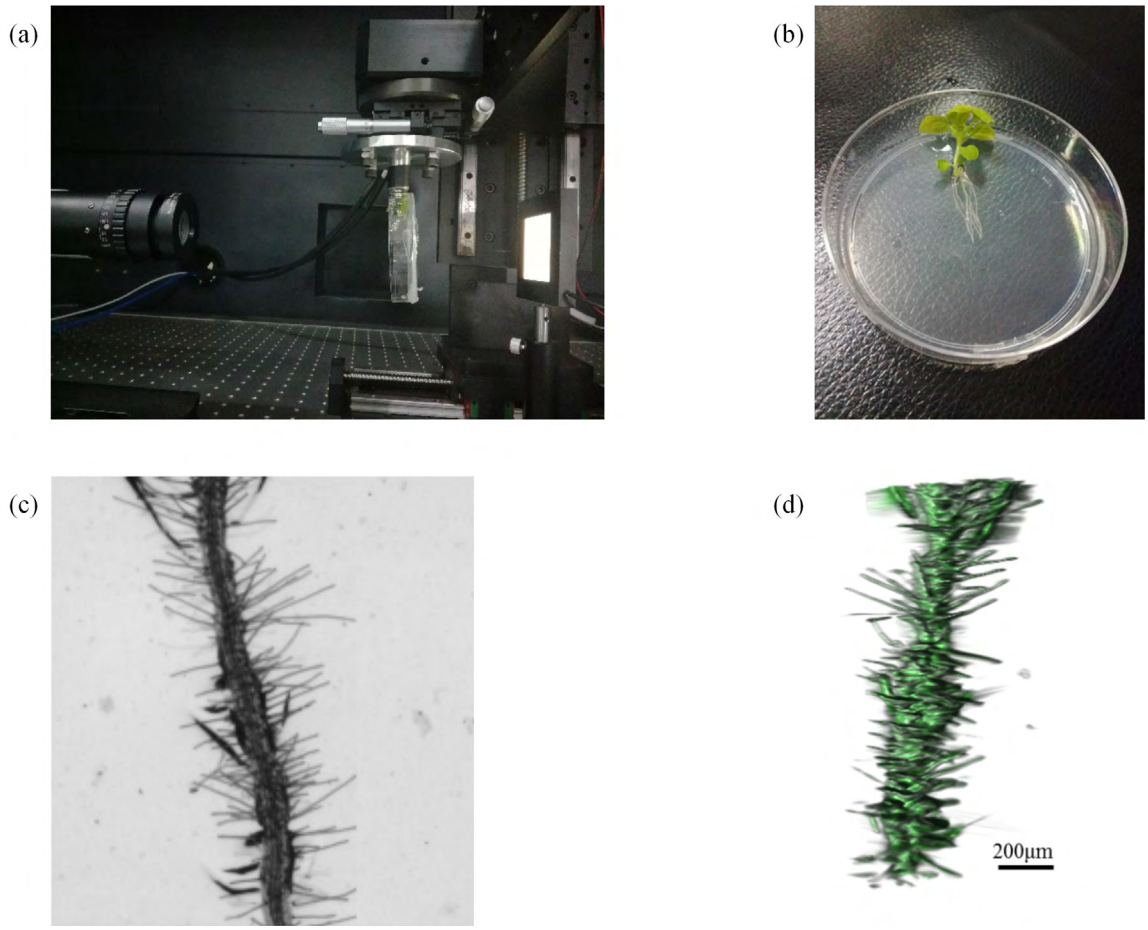

FIGURE 9. Tobacco root based on an applicable-potential demonstration. (a) Photograph of the sample fixation and experimental condition. (b)Picture of the tobacco plant. (c) and (d) One of the projection images and the reconstructed image of the TV regularized ART algorithm.

algorithm based limited-angle reconstruction was feasible and effective for the petri dish based sample fixation in *in vivo* optical projection tomography.

C. APPLICABLE-POTENTIAL DEMONSTRATION

In this section, the applicable-potential of the proposed sample fixation method combined with the limited-angle reconstruction algorithm was demonstrated by performing OPT imaging of tobacco roots. After the tobacco roots were affixed to the petri dish and held on the sample holder, 110 projection images were collected by rotating the sample with an interval of 1°. Fig. 9(a) shows the photograph of sample fixation, and Fig. 9(b) is the picture of the tobacco plant used in the experiment. One of the projection images is presented in Fig. 9(c), and the projection size was 2048×2048. In the experiment, only a part of the tobacco root was imaged due to the field of view limitation of the OPT system. The reconstructed image of the TV regularized ART algorithm by using the angular range of 110 degrees is shown in Fig. 9(d). From the reconstructed image, the density of the root hair can be clearly observed. This imaging experiment demonstrated the applicable-potential of the proposed sample fixation method and the TV regularized ART algorithm based limited-angle reconstruction framework.

IV. DISCUSSION AND CONCLUSION

In current OPT imaging, the specimen was immersed in index-matching fluid. In this case, the specimens could not survive or the survival time was too short, which was not suitable for longitudinal imaging. In this study, we first designed a new type of sample fixation method for *in vivo* OPT imaging. The specimen was embedded in a transparent gel in a petri dish, and the dish was then affixed to the rotational stage of our homemade OPT system. Due to the limitation of geometry of the petri dish, this fixation method induces a problem of insufficient measurements. The angles parallel to or nearly parallel to the top surface of the dish cannot be acquired. To address this problem, we utilized the TV regularized based limited-angle ART reconstruction framework. In this framework, the pixel vertex driven model (PVDM) was applied to parallel-beam OPT as the projection model. The total variation (TV) regularization combined with the algebraic reconstruction technique was used as the reconstruction algorithm to explore the impact of different angular ranges on the quality of reconstructed images. First, we performed

several simulations on a modified Shepp-Logan model to verify the feasibility of the limited-angle reconstruction framework. It indicated that the quality of reconstructed images became worse as the angular range was reduced. A reasonable image could be reconstructed when the angular range was down to as low as 130 degrees.

Second, we further evaluated the feasibility and universality of the proposed sample fixation method and TV regularized ART based reconstruction framework with two groups of biological samples. We found that detailed information could be observed when the angular range was no smaller than 140 degrees, and acceptable performance could be achieved when the angular range was larger than 110 degrees. Finally, the applicable-potential of the proposed sample fixation method and TV regularized ART based reconstruction framework was well demonstrated by the tobacco root based on *in vivo* OPT.

The sample fixation method proposed here can reduce the damage to the specimen and be more conducive to realization in *in vivo* OPT imaging and longitudinal studies. However, this method has some limitations. It is only suitable for organisms that have good ability of light transmission, such as nematodes, *Arabidopsis* pupae or larvae, and tobacco roots. For mouse embryos, *Drosophila* adults, and *Arabidopsis* horns, these non-transparent samples are not suitable. In addition, this method is only for organisms grown on solid media, and organisms such as zebrafish are not suitable. The petri dish used in this experiment is a flat, cylindrical shape, and the collected data are angularly limited. Specially customized petri dishes with lower margins can be fabricated in the future. Such petri dishes would not affect the normal growth of the organism, so that we can collect projection images from larger angular ranges, which would further improve the quality of the reconstructed image. The reconstruction framework used here had basically met the requirements. However, the algorithm is not specifically proposed for the limited-angle reconstruction problems. Better optimization algorithms are needed to improve the quality of the reconstructed images and obtain more suitable results.

In conclusion, this paper proposed a novel sample fixation method and a TV regularized based ART reconstruction framework for limited-angle for *in vivo* OPT. We explored the feasibility and demonstrated the applicable-potential with simulations and imaging experiments based on biological samples. We believe that this attempt will facilitate the development of limited-angle based on *in vivo* OPT.

ACKNOWLEDGMENT

Nan Wang and Duofang Chen contributed equally to this work

REFERENCES

[1] E. Osmanagic, A. L. Sukstanskii, J. D. Quirk, J. C. Woods, R. A. Pierce, M. S. Conradi, E. R. Weibel, and D. A. Yablonskiy, "Quantitative assessment of lung microstructure in healthy mice using an MR-based ^{3}He lung morphometry technique," *J. Appl. Physiol.*, vol. 109, no. 6, pp. 1592–1599, Dec. 2010.

[2] S. Zhu, J. Tian, G. Yan, C. Qin, and J. Feng, "Cone beam micro-CT system for small animal imaging and performance evaluation," *Int. J. Biomed. Imag.*, vol. 2009, May 2009, p. 960573.

[3] J. Thiesse, E. Namati, J. C. Sieren, A. R. Smith, J. M. Reinhardt, E. A. Hoffman, and G. McLennan, "Lung structure phenotype variation in inbred mouse strains revealed through *in vivo* micro-CT imaging," *J. Appl. Physiol.*, vol. 109, no. 6, pp. 1960–1968, Dec. 2010.

[4] B. Mehadji, Y. Ahmed, and J.-P. Berteau, "A novel approach for computing 3D mice distal femur properties using high-resolution micro-computed tomography scanning," *Micron*, vol. 121, pp. 1–7, Jun. 2019.

[5] A. Tsuda, N. Filipovic, D. Haberthür, R. Dickie, Y. Matsui, M. Stampanoni, and J. C. Schittny, "Finite element 3D reconstruction of the pulmonary acinus imaged by synchrotron X-ray tomography," *J. Appl. Physiol.*, vol. 105, no. 3, pp. 964–976, Sep. 2008.

[6] S. Meissner, L. Knels, C. Schnabel, T. Koch, and E. Koch, "Three-dimensional Fourier domain optical coherence tomography *in vivo* imaging of alveolar tissue in the intact thorax using the parietal pleura as a window," *J. Biomed. Opt.*, vol. 15, no. 1, Jan./Feb. 2010, Art. no. 016030.

[7] H. Yi, P. Jiao, X. Li, J. Peng, and X. He, "Three-way decision based reconstruction frame for fluorescence molecular tomography," *J. Opt. Soc. Amer. A, Opt. Image Sci.*, vol. 35, no. 11, pp. 1814–1822, Nov. 2018.

[8] W. M. Kuebler, K. Parthasarathi, J. Lindert, and J. Bhattacharya, "Real-time lung microscopy," *J. Appl. Physiol.*, vol. 102, no. 3, pp. 1255–1264, Mar. 2007.

[9] T. Abraham, J. A. Hirota, S. Wadsworth, and D. A. Knight, "Minimally invasive multiphoton and harmonic generation imaging of extracellular matrix structures in lung airway and related diseases," *Pulmonary Pharmacol. Therapeutics*, vol. 24, no. 5, pp. 487–496, Oct. 2011.

[10] R. G. Nava, W. Li, A. E. Gelman, A. S. Krupnick, M. J. Miller, and D. Kreisel, "Two-photon microscopy in pulmonary research," *Seminars Immunopathology*, vol. 32, no. 3, pp. 297–304, Sep. 2010.

[11] J. Sharpe, U. Ahlgren, P. Perry, B. Hill, A. Ross, J. Hecksher-Sørensen, R. Baldock, and D. Davidson, "Optical projection tomography as a tool for 3D microscopy and gene expression studies," *Science*, vol. 296, no. 5567, pp. 541–545, 2002.

[12] A. Arranz, D. Dong, S. Zhu, M. Rudin, C. Tsatsanis, J. Tian, and J. Ripoll, "Helical optical projection tomography," *Opt. Express*, vol. 21, no. 22, pp. 25912–25925, Nov. 2013.

[13] D. Dong, S. Zhu, C. Qin, V. Kumar, J. V. Stein, S. Oehler, C. Savakis, J. Tian, and J. Ripoll, "Automated recovery of the center of rotation in optical projection tomography in the presence of scattering," *IEEE J. Biomed. Health Informat.*, vol. 17, no. 1, pp. 198–204, Jan. 2013.

[14] H. Meyer, "*In vivo* optical projection tomography in biological model organisms," Erasmus Univ. Rotterdam, Dordrecht, The Netherlands, Tech. Rep., Jan. 2010, pp. 50–52.

[15] M. Rieckher, U. J. Birk, H. Meyer, J. Ripoll, and N. Tavernarakis, "Microscopic optical projection tomography *in Vivo*," *PLoS One*, vol. 6, no. 4, Apr. 2011, Art. no. e18963.

[16] A. M. Petzold, V. M. Bedell, N. J. Boczek, J. J. Balciunas, K. J. Clark, and S. C. Ekker, "SCORE imaging: Specimen in a corrected optical rotational enclosure," *Zebrafish*, vol. 7, no. 2, pp. 149–154, Jun. 2010.

[17] A. Bassi, L. Fieramonti, C. D'Andrea, M. Mione, and G. Valentini, "*In vivo* label-free three-dimensional imaging of zebrafish vasculature with optical projection tomography," *J. Biomed. Opt.*, vol. 16, no. 10, Oct. 2011, Art. no. 100502.

[18] A. Bassi, L. Fieramonti, C. D'Andrea, G. Valentini, R. Cubeddu, S. De Silvestri, G. Cerullo, E. Foglia, and F. Cotelli, "*In vivo* imaging of zebrafish from embryo to adult stage with optical projection tomography," *Proc. SPIE*, vol. 8593, Mar. 2013, Art. no. 85930A.

[19] M. Jiang and G. Wang, "Convergence of the simultaneous algebraic reconstruction technique (SART)," *IEEE Trans. Image Process. Publ. IEEE Signal Process. Soc.*, vol. 12, no. 8, pp. 957–961, Aug. 2003.

[20] E. Y. Sidky, C.-M. Kao, and X. Pan, "Accurate image reconstruction from few-views and limited-angle data in divergent-beam CT," *J. X-Ray Sci. Technol.*, vol. 14, no. 2, pp. 119–139, 2006.

[21] Y. Lu, J. Zhao, and G. Wang, "Few-view image reconstruction with dual dictionaries," *Phys. Med. Biol.*, vol. 57, no. 1, pp. 173–189, 2012.

[22] Z. Chen, X. Jin, L. Li, and G. Wang, "A limited-angle CT reconstruction method based on anisotropic TV minimization," *Phys. Med. Biol.*, vol. 58, no. 7, pp. 2119–2141, 2013.

[23] D. Yi, W. Xiangang, X. Xincheng, and W. Zhouping, "Evaluation of hybrid SART+OS+TV iterative reconstruction algorithm for optical-CT gel dosimeter imaging," *Phys. Med. Biol.*, vol. 61, no. 24, pp. 8425–8439, Dec. 2016.

[24] X. Luo, W. Yu, and C. Wang, "An image reconstruction method based on total variation and wavelet tight frame for limited-angle CT," *IEEE Access*, vol. 6, pp. 1461–1470, 2018.
[25] P. Bao, J. Zhou, and Y. Zhang, "Few-view CT reconstruction with group-sparsity regularization," *Int. J. Numer. Methods Biomed. Eng.*, vol. 34, no. 9, p. e3101, Sep. 2018.
[26] Y. Zhang, H.-P. Chan, B. Sahiner, J. Wei, M. M. Goodsitt, L. M. Hadjiiski, J. Ge, and C. Zhou, "A comparative study of limited-angle cone-beam reconstruction methods for breast tomosynthesis," *Med. Phys.*, vol. 33, no. 10, pp. 3781–3795, 2006.
[27] M. Rantala, S. Vanska, S. Jarvenpaa, M. Kalke, M. Lassas, J. Moberg, and S. Siltanen, "Wavelet-based reconstruction for limited-angle X-ray tomography," *IEEE Trans. Med. Imag.*, vol. 25, no. 2, pp. 210–217, Feb. 2006.
[28] M. K. Cho, H. Youn, S. Y. Jang, and H. K. Kim, "Cone-beam digital tomosynthesis for thin slab objects," *NDT E Int.*, vol. 47, pp. 171–176, Apr. 2012.
[29] H. Gao, L. Zhang, Z. Chen, Y. Xing, and J. Cheng, "An extrapolation method for image reconstruction from a straight-line trajectory," in *Proc. IEEE Nucl. Sci. Symp. Conf. Rec.*, Oct./Nov. 2007, p. 5.
[30] J. K. Choi, B. Dong, and X. Zhang, "Limited tomography reconstruction via tight frame and simultaneous sinogram extrapolation," *J. Comput. Math.*, vol. 34, no. 6, pp. 575–589, 2016.
[31] H. Zhang, L. Li, L. Wang, Y. Sun, B. Yan, A. Cai, and G. Hu, "Computed tomography sinogram inpainting with compound prior modelling both sinogram and image sparsity," *IEEE Trans. Nucl. Sci.*, vol. 63, no. 5, pp. 2567–2576, Oct. 2016.
[32] G.-H. Chen, J. Tang, and S. Leng, "Prior image constrained compressed sensing (PICCS): A method to accurately reconstruct dynamic CT images from highly undersampled projection data sets," *Med. Phys.*, vol. 35, no. 2, pp. 660–663, 2008.
[33] T. Heußer, M. Brehm, L. Ritschl, S. Sawall, and M. Kachelrieß, "Prior-based artifact correction (PBAC) in computed tomography," *Med. Phys.*, vol. 41, no. 2, Feb. 2014, Art. no. 021906.
[34] E. J. Candès, J. Romberg, and T. Tao, "Robust uncertainty principles: Exact signal reconstruction from highly incomplete frequency information," *IEEE Trans. Inf. Theory*, vol. 52, no. 2, pp. 489–509, Feb. 2006.
[35] M. Jiang and G. Wang, "Convergence studies on iterative algorithms for image reconstruction," *IEEE Trans. Med. Imag.*, vol. 22, no. 5, pp. 569–579, May 2003.
[36] R. Gordon, R. Bender, and G. T. Herman, "Algebraic reconstruction techniques (ART) for three-dimensional electron microscopy and X-ray photography," *J. Theor. Biol.*, vol. 29, no. 3, p. 471, 1970.
[37] H. Yu and G. Wang, "Compressed sensing based interior tomography," *Phys. Med. Biol.*, vol. 54, no. 9, pp. 2791–2805, May 2009.
[38] T. Gomi, R. Sakai, M. Goto, H. Hara, Y. Watanabe, and T. Umeda, "Evaluation of digital tomosynthesis reconstruction algorithms used to reduce metal artifacts for arthroplasty: A phantom study," *Phys. Medica*, vol. 42, pp. 28–38, Oct. 2017.
[39] Y. Long, J. A. Fessler, and J. M. Balter, "3D forward and back-projection for X-ray CT using separable footprints," *IEEE Trans. Med. Imag.*, vol. 29, no. 11, pp. 1839–1850, Nov. 2010.
[40] Z. Wang, A. C. Bovik, H. R. Sheikh, and E. P. Simoncelli, "Image quality assessment: From error visibility to structural similarity," *IEEE Trans. Image Process.*, vol. 13, no. 4, pp. 600–612, Apr. 2004.
[41] S. Zhu, D. Dong, U. J. Birk, M. Rieckher, N. Tavernarakis, and X. Qu, "Automated motion correction for *in vivo* optical projection tomography," *IEEE Trans. Med. Imag.*, vol. 31, no. 7, pp. 1358–1371, Jul. 2012.

NAN WANG received the B.S. degree from Tianjin Polytechnic University, Tianjin, China, in 2017. She is currently pursuing the Ph.D. degree with the School of Life Science and Technology, Xidian University. Her research interest includes dual-modality imaging of optical-Raman projection tomography.

DUOFANG CHEN received the Ph.D. degree in signal and information processing from Xidian University, Xi'an, China, in 2009, where she is currently an Associate Professor with the School of Life Science and Technology. Her research interests include tomography reconstruction and signal processing algorithms in fNIR imaging.

DAN CHEN received the B.S. degree from Central China Normal University, Wuhan, China, in 2002, and the Ph.D. degree from Wuhan University, Wuhan, in 2008. She is currently an Associate Professor with the School of Life Science and Technology, Xidian University, Xi'an, China. Her research interests include gene coding probes and tumor biology.

CUIPING BAO received the B.S. degree from the China University of Petroleum, Qingdao, China, in 2015, and the M.S. degree from the School of Life Science and Technology, Xidian University, in 2018. Her research interest includes optical projection tomography imaging.

JIMIN LIANG received the Ph.D. degree from Xidian University, in 2000. He is currently a Professor with Xidian University, Xi'an, China. His research interests include image processing and analysis, and multimodality molecular imaging.

XUELI CHEN received the B.S. degree in biomedical engineering and the Ph.D. degree in pattern recognition and intelligent system from Xidian University, Xi'an, China, in 2007 and 2012, respectively, where he is currently a Professor with the School of Life Science and Technology. From 2015 to 2017, he was a Postdoctoral Researcher with Purdue University. His research interest includes multi-scale and multi-modality biophotonics imaging and its applications. He has authored or coauthored more than 60 peer-reviewed journal papers on these topics. He is currently a member of OSA and SPIE.

SHOUPING ZHU received the B.S. degree in biomedical engineering and the M.S. degree in signal and information processing from Xidian University, Xi'an, China, in 2004 and 2007, respectively, and the Ph.D. degree in pattern recognition and intelligent systems from the Chinese Academy of Sciences, Beijing, China, in 2010. He is currently a Professor with the School of Life Science and Technology, Xidian University. His research interests include multi-modality medical imaging systems, micro-CT imaging, PET imaging, optical imaging, and tomography reconstruction with GPU.